Article

The Oligomerization Landscape of Histones

Haiqing Zhao[1,2], David Winogradoff[3,4], Yamini Dalal[5,*], and Garegin A. Papoian[1,3,6,**]

[1]Biophysics Program, Institute for Physical Science and Technology, University of Maryland, College Park, MD 20742, USA
[2]Present address: Department of Systems Biology, Columbia University, New York, NY 10032, USA
[3]Chemical Physics Program, Institute for Physical Science and Technology, University of Maryland, College Park, MD 20742, USA
[4]Present address: Department of Physics, Center for the Physics of Living Cells, University of Illinois at Urbana-Champaign, Urbana, IL 61801, USA
[5]Laboratory of Receptor Biology and Gene Expression, National Cancer Institute, National Institutes of Health, Bethesda, MD 20892, USA
[6]Department of Chemistry and Biochemistry, University of Maryland, College Park, MD 20742, USA
[*]Correspondence: dalaly@mail.nih.gov
[**]Correspondence: gpapoian@umd.edu

ABSTRACT In eukaryotes, DNA is packaged through nucleosomes. Each nucleosome is typically centered around an octameric histone protein core: one central tetramer plus two separate dimers. Studying the assembly mechanisms of histones is essential for understanding the dynamics of entire nucleosomes and higher-order DNA packaging. Here we investigate the canonical histone assembly and that of the centromere-specific histone variant CENP-A using molecular dynamics simulations. We quantitatively characterize their thermodynamical and dynamical features, showing that the canonical H3 tetramer exhibits large instability around the central interface manifested *via* a swiveling motion of two halves, supporting the recently observed DNA handedness flipping of the tetrasome. In contrast, the variant CENP-A encodes a distinctive stability to its tetramer with a rigid but twisted interface compared to the crystal structure, implying the diverse structural possibilities of the histone variant. Interestingly, the observed tetramer dynamics alter significantly and appear to reach a new dynamics balance when H2A/H2B dimers are present. In all, these data reveal key mechanistic insights and structural details for the assembly of canonical and variant CENP-A histone tetramers and octamers, providing theoretical quantifications and physical interpretations for longstanding and recent experimental observations.

INTRODUCTION

Eukaryotes wrap their DNA around histone proteins constituting the fundamental unit of chromatin, the nucleosome. Inside each nucleosome, histones typically exist as an octamer, composed of a central tetramer $(H3/H4)_2$ plus one H2A/H2B dimer on either side (1). Nucleosomes dynamically dissociate and re-associate in chromatin structure for fundamental biological processes like DNA transcription, replication, or repair. By initiating nucleosome assembly through forming a tetrasome with DNA, the histone tetramer serves as the structural basis for nucleosomal or chromatin dynamics (2, 3). Thus, it is crucial to elucidate the dynamics of histone tetramers, which are key intermediates along nucleosome assembly and disassembly pathways. Recent single-molecule experiments studied the spontaneous flipping behavior of DNA handedness of the tetrasome, finding that iodoacetamide-treated residue mutations on the tetramer can cause the enhanced flexibility and faster superhelical flipping kinetics of the wrapped DNA (4–6). Therefore, a deep molecular understanding of histone tetramer dynamics is not only essential to understanding subnucleosomal or nucleosomal assembly, but may also suggest innovative pathways for higher-order DNA packaging.

The centromere-specific histone H3 variant, Centromere Protein A (CENP-A), has been extensively studied in recent decades for its significant functional role as the epigenetic mark of the centromere and ensuring proper chromosome separation during cell division (7–12) and for its unique structural dynamics, (13–17) particularly dissecting the dominant structure of CENP-A nucleosomes (18–23), and their association with kinetochore partners (24–28). Unlike canonical H3 nucleosomes, CENP-A-containing nucleosomes follow a different assembly pathway *via* the unique chaperone HJURP (29–33). Also, in cancer cells CENP-A is over-expressed and the redundant CENP-A can localize into ectopic (*i.e.* non-centromeric) regions *via* alternative pathways (15, 34, 35). Thus, one outstanding question is whether CENP-A, in normal cells, can be efficiently regulated to avoid ectopic delivery. Another related question is whether replacing canonical H3 with CENP-A alters its physical properties and overall dynamics.

Conflicting studies have suggested that: (1) *in vitro* chromatography and deuterium exchange experiments (36) indicate that the soluble CENP-A/H4 forms a more compact and rigid tetramer than the conventional H3 complex (18, 36); partially truncated CENP-A tetramers adopt compact conformations in crystals and in solution; (37) (2) CENP-A- and H3-containing nucleosomes have nearly identical crystal structures(38, 39), and (3) recent compuational and experimental studies reveal that CENP-A dimers(40) and nucleosomes(41, 42) are more flexible than their canonical H3 counterparts. On the other hand, canonical histone tetramers present consistent crystal structures in different molecular contexts, including as a tetramer in a nucleosome (1, 43), in an octamer(44–46), and in complexes with chaperones such as FACT (47), Spt2 (48), TONSL and MCM2 (49, 50). Early size-exclusion chromatography experiments demonstrate that there is a dynamic equilibrium between two H3/H4 dimers and an assembled tetramer (51, 52), and this equilibrium is responsive to changes in ionic strength (53). Through Electron Paramagnetic Resonance (EPR) spectroscopy, a previous study shows that the histone tetramer exhibits greater structurally heterogeneity on its own than when sequestered in the octamer (54). However, dynamical structural details that would reveal the mechanisms governing the observed properties are not readily available to existing experimental techniques. Here we apply computational modeling to study both H3- and CENP-A-oligomers trying to provide a comprehensive theoretical quantification that can explain and unify these experimental observations that might seem incompatible.

Among computational approaches, molecular dynamics (MD) simulations are able to capture mechanistic details at the molecular level, complementing experimental approaches. Previously, we used atomistic MD to reveal that the CENP-A nucleosome exhibits greater flexibility than the canonical nucleosome around their native states (41), and its dynamics can be modulated by internal modifications (17). Combining coarse-grained, atomistic simulations and *in vivo* mutation experiments, we reported that the CENP-A dimer is structurally variable, and chaperone HJURP prevents the promiscuous mis-assembly of the CENP-A dimer, protecting it from binding with other proteins (40).

Building upon these findings, we performed coarse-grained MD simulations using the AWSEM model (55) (CG-AWSEM; *i.e.* 3-beads per amino acid) to investigate the assembly mechanisms of histone tetramers and asked whether histones CENP-A and H3 differ at the tetramer/octamer level. We computed the association free energy of two dimers forming a tetramer, finding that CENP-A dimers form a more compact and stable tetramer with a more favorable free energy, while the landscape of the H3 tetramer is more rugged, indicating its structural lability. In particular, simulations starting from pre-assembled tetramers reveal swiveling motion around the H3 tetramer interface. Furthermore, histone octamer simulations suggest that the addition of H2A/H2B dimers gently restrains the internal rotation of the H3 tetramer while leading the CENP-A tetramer to adopt multiple conformational states, demonstrating a significant incongruence between the preferred structures of the CENP-A tetramer versus the octamer. Finally, we put forward a model for canonical and variant histone assembly and propose that the CENP-A tetramer may serve as a critical sequestration channel, preventing the assembly of excess CENP-A into chromatin, thereby regulating CENP-A homeostasis *in vivo*.

MATERIALS AND METHODS

Initial structures

Initial configurations of canonical histone tetramer used in the simulation are all from the nucleosome crystal structures containing H3 (PDB: 1KX5 (43)). Initial configurations for CENP-A tetramer are obtained from CENP-A-containing nucleosome (PDB: 3AN2 (38)) and the αN-helices-truncated CENP-A tetramer crystal structure (PDB: 3NQJ (18)). We compared and overlaid the histone tetramer structures from different structural environments, as provided in Supporting Figure S3. Histone tails and DNA were not included in current study. All the sequences of simulated proteins are included in the Figure S4.

Simulation methods and trajectory analyses

In this work, we used Associative-memory, Water-mediated, Structure and Energy Model (AWSEM) to carry out computational simulations for both canonical and variant CENP-A histone tetramers and octamers. Details of AWSEM can be found in the SI and also in the original paper ref. 55. Since AWSEM is a model based on not only the physical interactions like hydrogen-bonding but also the structural-biasing potential terms, here we use the respective histone monomer structures to build up the biasing structural fragment memory database. Each fragment is from 3- to 12-residue long. It is important to note that no binding information between histone monomers or between dimers were provided to the force field. So, from this perspective, AWSEM is a predictive coarse-grained protein model with transferable force fields.

All simulations were performed in the large-scale atomic/molecular massively parallel simulator 2016 (LAMMPS 2016), using the Nosé-Hoover thermostat. We applied the umbrella-sampling together with replica-exchange (56) to enhance the phase space sampling for further free energy calculations. For instance, in the case of H3 dimers' association, two H3 dimers were put in the simulation with the distance between their centers-of-mass controlled by an umbrella constraint. A typical harmonic potential is used for this purpose as shown in Eq.(1), where k_R is the biasing strength and R_o is the controlled center distance

for each window. Here k_R = 5 kcal/mol/Å^2, and R_o ranges from 20 Å to 50 Å, averagely spaced by 1 Å. Simulations for each umbrella window, in total 30, were performed using ten replicas with temperatures linearly ranging from 280 K to 370 K. After the simulation reached convergence (see below and Supplemental Section 4), data from different windows were then collected together and we used weighted histogram analysis method (WHAM) (57) to calculate the PMFs and construct free-energy landscapes on different coordinates. A relevant Jacobian factor correction term, $k_BT\ln[4\pi R^2]$, was subtracted from the free energy calculation since a sampling space based on the distance R_{COM} makes unphysical contributions to the configurational partition function(58). The time step is set at 5 fs in all simulations. Each replica was run for 2 million steps. Exchanges between replicas were attempted every 400 steps. The first 0.5 million steps were not included for analysis to allow the systems to reach equilibration.

$$U_{umbrella} = \frac{1}{2}k_R(R - R_0)^2 \tag{1}$$

Separately, ten independent constant temperature simulations were carried out for tetramers (H3/H4)$_2$ and (CENP-A/H4)$_2$, with 30 million timesteps each and 300 million steps in total (1500 ns in the coarse-grained timescale). Weak biases in the form of harmonic potential (k = 0.02 kcal/mol/Å^2) were applied between two monomers in a dimer and between two dimers in a tetramer to control the overall concentration of monomers. Simulations and analyses for H3 and CENP-A tetramers that exclude αN helices are performed using the same setup. Similarly, octamer simulations for (H3/H4)$_2$ and (CENP-A/H4)$_2$ with two (H2A/H2B)s were run for 10 million timesteps with a totaling 100 million timesteps for each octamer system. Simulations were performed in a 200-Å-long cubic box with periodic boundary conditions. Trajectories were combined for later data analysis after removing the first 10 ns in every run to account for thermal equilibration. Note that the coarse-graining timescale cannot be directly converted into real time unit since it could be 10 times larger than that in the fully atomistic MD simulations(59). The convergences of all simulations were verified by the root-mean-squared inner-product (RMSIP) analysis, which are provided in the Supplemental Section 4.

All the trajectory analyses in this work, including the calculations of root-mean-square deviations (RMSD), radius-of-gyration (R_g), distances (R), dihedral angles θ, Q values, and contact analysis, were based on the Cα coordinates. More analyzing details including error analyses are included in the Supplemental Section 2 and 3.

RESULTS

Binding free energy of two dimers forming a tetramer

Motivated by the previous observation of CENP-A dimer's flexibility (40) compared with the canonical counterpart, we first investigated the formation of tetramers from two canonical H3 and CENP-A dimers. *Via* a mixed enhanced sampling methodology that couples replica-exchange with umbrella-sampling, we mapped their corresponding binding free energy landscapes. The calculated free energy profiles (FEP) were projected into two reaction coordinates: the distance between centers-of-mass of the two dimers R_{COM} and another order parameter that quantifies the nativeness of the binding interface between the dimers, $Q_{interface}$. $Q_{interface}$ is the fraction of native interface contacts, defined as, $\frac{1}{n}\sum_{i<j-2}\exp\left[-\frac{\left(r_{ij}-r_{ij}^{native}\right)^2}{2\sigma_{ij}^2}\right]$, where n is the total number of contacts, r_{ij} is the distance between the Cα atoms of residues i and j, and σ_{ij} is given as $\sigma_{ij} = (1 + |i - j|^{0.15})$. Q ranges from 0 to 1, where no common contacts between a conformation and the native state corresponds to 0 and complete similarity of contacts corresponds to 1. Here the $Q_{interface}$ calculations were conducted with respect to the tetramer interface from the corresponding nucleosomes containing canonical H3 and variant CENP-A (PDB: 1KX5 (43) and 3AN2 (38)).

As seen in Figure 1, the binding free energy landscape for H3/H4 dimers is relatively rugged with multiple energy minima, at $Q_{interface}$ = 0.4, 0.1~0.2, and 0.0; R_{COM} of 29 Å, 32~33 Å and 38 Å in the other dimension (Figure 1A). These minima are relatively flat compared to that of CENP-A, occupying a large portion of configuration space described in terms of R_{COM} and $Q_{interface}$, indicating larger structural heterogeneity of (H3/H4)$_2$ with a broad ensemble of accessible conformations. This result is consistent with the experimental observation that histone H3 tetramer is unstable at moderate ionic strengths, determined by guanidinium-induced denaturation (51). On the other hand, the two CENP-A/H4 dimers present a deep, well-funneled association free energy landscape (Figure 1B), with the minimum at R_{COM} = 29 Å, $Q_{interface}$ = 0.4, suggesting that there is a thermodynamically favorable binding state for the tetramer (CENP-A/H4)$_2$.

To further quantify and compare the binding free energies for H3/H4 and CENP-A/H4, we projected two computed FEPs along one dimension, R_{COM}, after aligning both the converged FEs at the far-end to zero, at which we assume there is no interaction between the two dimers (*i.e.* when R_{COM} > 50 Å). Figure 2 presents the free energy profile as a function of the distance between the COMs of two H3 dimers or CENP-A dimers, demonstrating that the FEP minima for (CENP-A/H4)$_2$ and

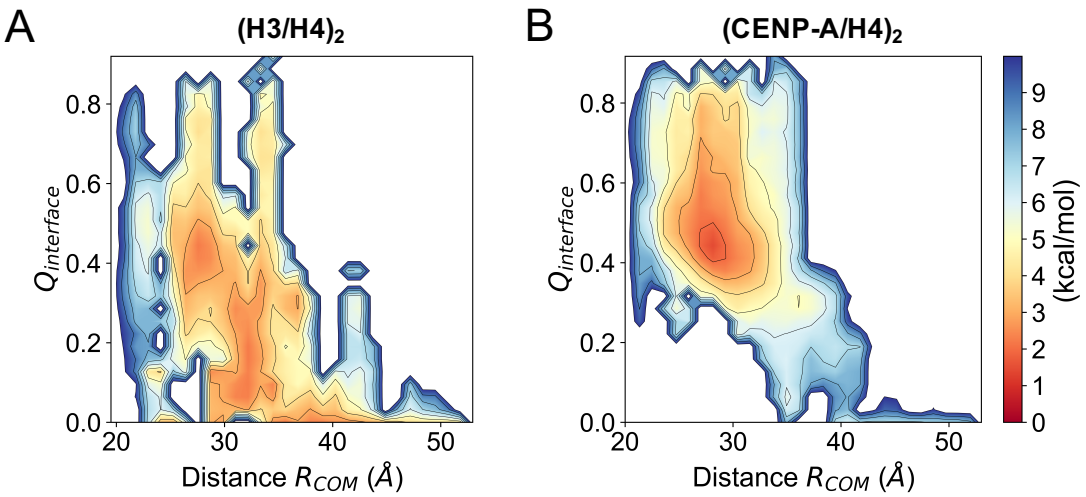

Figure 1: **The binding free energy landscapes of the H3 and CENP-A tetramers.** Two-dimensional free energy profiles are mapped as a function of the distance between two interacting dimers R_{COM} and of the quantification of the nativeness of their binding interface $Q_{interface}$, for $(H3/H4)_2$ (A) and $(CENP\text{-}A/H4)_2$ (B).

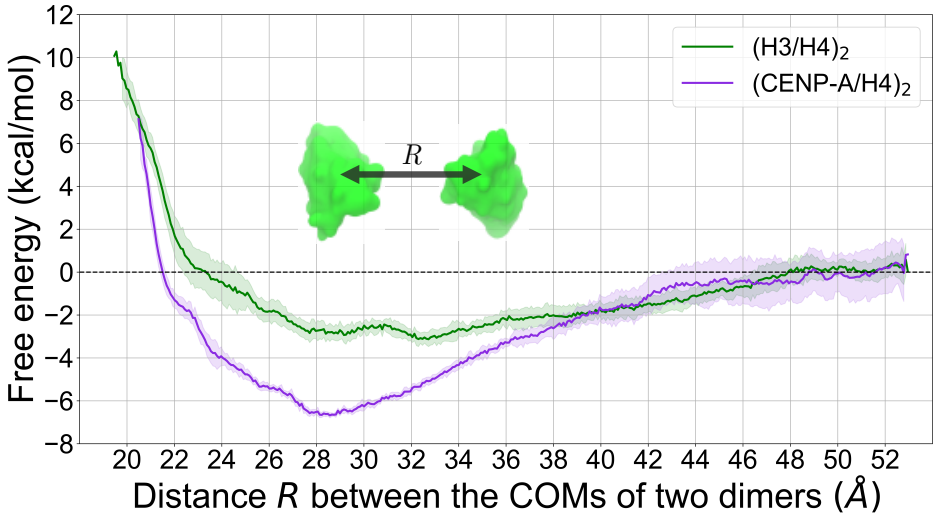

Figure 2: **$(CENP\text{-}A/H4)_2$ has a deeper free energy profile than $(H3/H4)_2$.** The potential of mean force (PMF) along the distance R between histone dimers is deeper for $(CENP\text{-}A/H4)_2$ (purple) than for $(H3/H4)_2$ (green). R is measured from the center-of-mass (COM) of one dimer to the other. The shaded areas illustrate the standard deviations of the curves.

$(H3/H4)_2$ are appropriately at −7 kcal/mol and −3 kcal/mol. Since the overall FEP curve of CENP-A dimers is deeper, we expect that, in the absence of DNA and other histone proteins, CENP-A/H4 dimers can more readily assemble into a tetramer than H3/H4 dimers. Furthermore, the free energy minimum is located at a distance of ∼28 Å between dimers of CENP-A/H4 and at ∼32 Å between dimers of H3/H4 (Figure 2), indicating that the thermodynamically favored CENP-A tetramer is more compact than the H3 tetramer. This result agrees quantitatively with previous SAXS measurements that found the CENP-A tetramer to be substantially more compacted relative to their H3 counterparts (18). Also, Banks and Gloss used far-UV circular dichroism to measure the folding and unfolding kinetics of $(H3/H4)_2$(52) experimentally. The free energy of the dimer-tetramer reaction they obtained is −2.6 kcal/mol. Our computed minimum, at −3 ± 0.2 kcal/mol, is in qualitative agreement with their

experimentally measured data. Overall, these free energy calculations suggest that the CENP-A/H4 homotypic tetramer is thermodynamically more stable, and more compact, than that of H3/H4. Additional free energy profiles projected on other reaction coordinates, both one-dimensional and two-dimensional, are provided in the SI (Supplementary Figures S4 and S5).

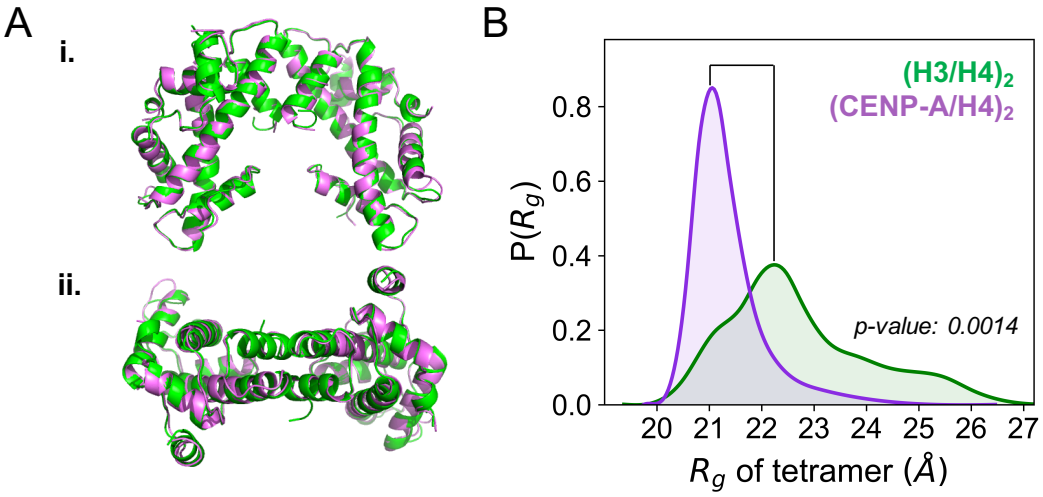

Figure 3: **(CENP-A/H4)$_2$ is more compact than (H3/H4)$_2$.** (A) The initial conformations of the H3 tetramer (green) and CENP-A tetramer (purple) were taken from their nucleosome crystal structures (PDB IDs: 1KX5 and 3AN2). Lateral view (i) and top view (ii) of aligned structures are displayed. (B) The CENP-A tetramer has a smaller radius-of-gyration R_g than the H3 tetramer, with a narrower distribution.

Tetramer geometries and the swiveling dynamics

To further explore the intrinsic dynamics of histone tetramers, we performed microsecond-scale continuous constant temperature CG-AWSEM simulations for CENP-A and H3 tetramers, starting from pre-assembled conformations taken from the central tetramers of the corresponding octameric nucleosome crystal structures (Figure 3A). Other structures from octamer or chaperone-tetramer complexes could have been used as well because the overall structures of the tetramer are nearly identical despite divergent crystallization conditions (Supplementary Figure S3). Overall, our results obtained from these continuous simulations were broadly consistent with the above enhanced sampling simulations, and they provide important dynamics insights. We present here some of the most salient observations; additional analyses including the principle component analysis (PCA) and other structural quantities including the root-mean-square deviation (RMSD), R_{COM}, and $Q_{interface}$ can be found in the SI (Supplementary Figure S9, S7A,B,C).

To quantify the molecules' degree of compaction, we calculated the radius of gyration of tetramer, defined as $R_g = \sqrt{\frac{1}{N^2}\sum_{i=1,i<j}^{N}(\boldsymbol{r_i}-\boldsymbol{r_j})^2}$, where N is the total number of residues and $\boldsymbol{r_i}$ are the coordinates of ith residue. Figure 3B shows that the average R_g for (CENP-A/H4)$_2$ is 21 ± 0.7 Å and 23 ± 1.4 Å for (H3/H4)$_2$, implying that (CENP-A/H4)$_2$ samples more compact geometries with less R_g fluctuations. The R_g distribution of (CENP-A/H4)$_2$ is unimodal, with a dominant central peak, while the H3 tetramer R_g samples a much broader distribution (Figure 3B), consistent with the above free energy calculations (Figure 2). Moreover, the mean value difference between the two systems in our simulation matches the previous experimental data, where Black *et al.* measured that the CENP-A tetramer complex chromatographs as a single species with a Stokes radius of 28 Å, smaller than that of H3/H4, 30.5 Å(36). Together, these results suggest that the CENP-A tetramer is more closely packed, structurally more well-defined than the canonical H3 tetramer.

In recent magnetic tweezer experiments, the DNA of H3-containing tetrasomes were observed to flip between left- and right-handed superhelically-wound states(5, 6), which may be initiated by conformational changes of the proteins inside. To better compare with these experiments, we examined the overall orientation of the simulated tetramers by measuring the dihedral angle between the two composing dimers. We chose to measure the dihedral angle of the two H3 $\alpha 2$ helices (similarly for CENP-A), since they are the longest continuous structural component in each dimer molecule.

Our results demonstrate that, compared to (CENP-A/H4)$_2$, the two H3 dimers in (H3/H4)$_2$ occupy a range of orientations,

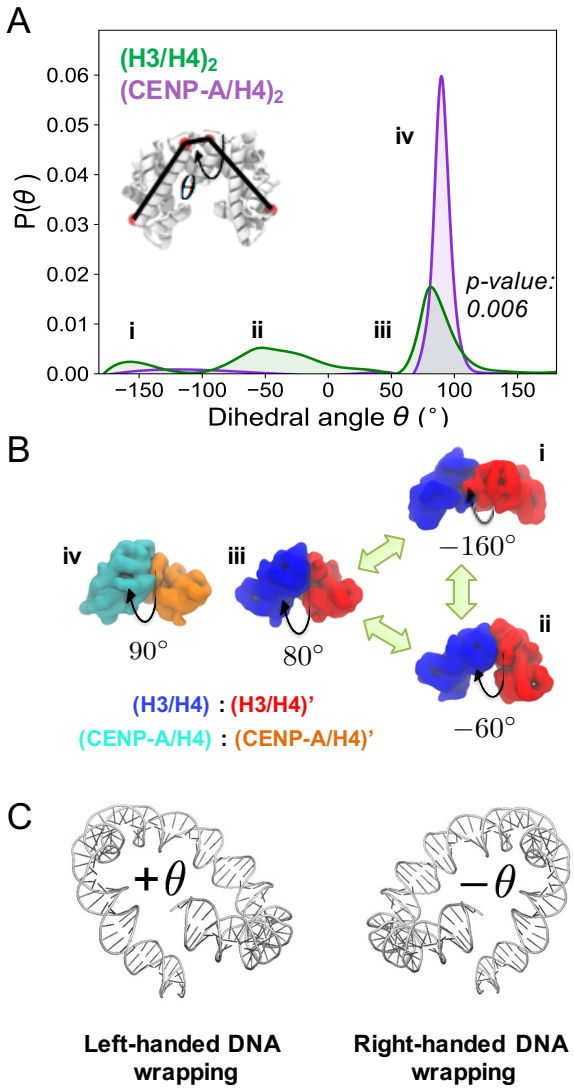

Figure 4: **The H3 tetramer swivels around its binding interface while the CENP-A tetramer remains relatively stable.** (A) The distribution for the dihedral angle between $\alpha 2$ helices features one prominent peak for $(\text{CENP-A/H4})_2$, and three smaller peaks for $(\text{H3/H4})_2$, indicating $(\text{CENP-A/H4})_2$ maintains a more fixed orientation than $(\text{H3/H4})_2$. (B) Representative conformations from each population are displayed. (C) Positive (+) and negative (−) dihedral angles of the histone tetramer measured here correspond to the left-handed and right-handed DNA superhelical wrapping in the tetrasome, respectively.

as indicatd by the distribution of the above-mentioned dihedral angle that includes three populations (Figure 4B): one positive and two negative, three distinct states in total (Figure 4A,B i,ii,iii). Furthermore, $(\text{H3/H4})_2$ frequently transits from one dihedral angle to another, undergoing swiveling motion around the binding interface (Supplemental Figure S8 and Supplemental Movie S1). The range of orientations for two histone dimers and its dynamical transition found in our simulations can explain the spontaneous flipping behavior of DNA handedness in the tetrasome as revealed in magnetic tweezer experiments (6). A positive dihedral angle of the tetramer would correspond to left-handed superhelically-wrapped DNA, and vice versa (Figure 4C).

In contrast, $(\text{CENP-A/H4})_2$ maintains a relatively fixed orientation, with no obvious rotational motions around the interface (Supplemental Movie S2). The dihedral angle between the scaffold helices is about 90° (Figure 4A,B iv), less than the angle measured in crystal structures of the CENP-A tetramer from the nucleosome or with chaperones (110°), implying a twisted interface geometry. Indeed, from the simulation snapshots, as well as other measurements including overall R_g and R_{COM} between dimers, the two CENP-A/H4 dimers seem to pack more closely together in a twisted orientation, presenting a compact tetramer. Moreover, we observe that, in the absence of DNA and other histones, both H3 and CENP-A histone tetramers prefer

not to occupy the same plane compared to the geometries of their respective nucleosome structures (Figure 4A). The $\alpha 2$ helices of CENP-A were found to be curved (Figure S15) as was also revealed from hydrogen exchange mass spectrometry (37). H3 $\alpha 2$ helices were also found to be curved (Figure S14). The curvature of $\alpha 2$ helices could be a result of the absence of surrounding DNA and bracketing H2A/H2B, which provide necessary topological support to the central tetramer.

Distinct dynamics at the tetrameric interface

To uncover the mechanistic basis for the observed difference in behavior between CENP-A and H3 tetramers, we then assessed whether it arises from the tetrameric interface (*i.e.* the interface between two dimers). We calculated $Q_{interface}$ for the continual simulations, referring to the native interface contacts from the crystal structure (PDB: 1KX5). The distribution for the CENP-A tetramer is centered at 0.5, while the same distribution for the H3 tetramer contains three peaks, with an average value of 0.2 (Figure S7B). This result implies that (CENP-A/H4)$_2$ forms a tetrameric interface that is better defined and more native-like compared to (H3/H4)$_2$. In the context of the DNA-free tetramer, the four-helix bundle of (CENP-A/H4)$_2$ which composes the tetrameric interface still maintains a well-connected and symmetric geometric arrangement (Figure 5B), despite some structural twisting. This is not found in the H3 tetramer case.

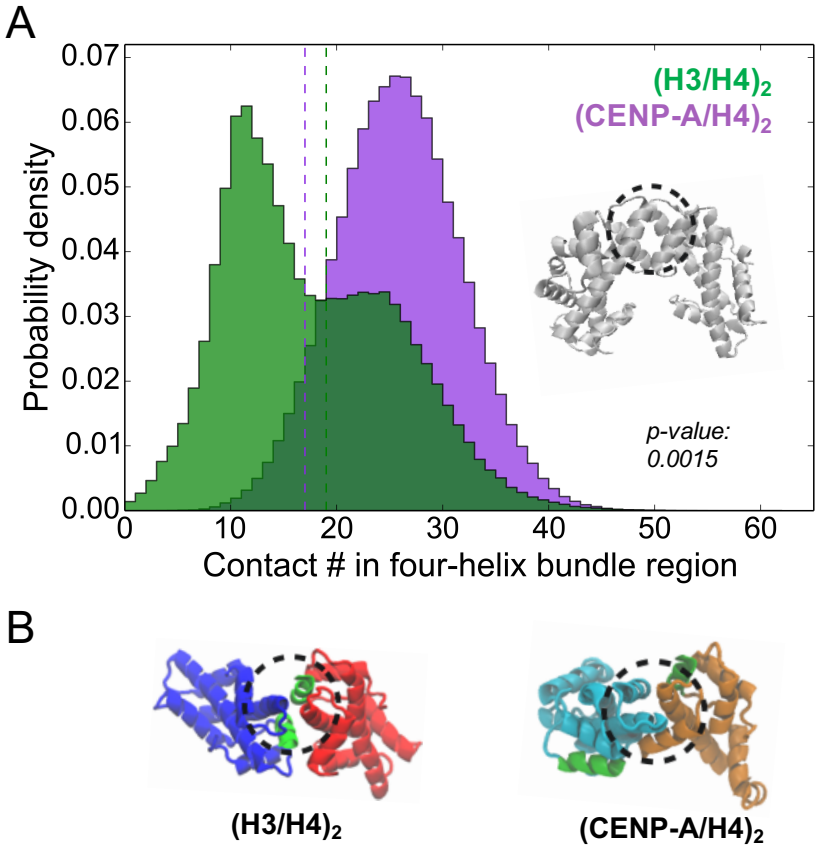

Figure 5: **(CENP-A/H4)$_2$ has a more stable four-helix bundle than (H3/H4)$_2$.** (A) (H3/H4)$_2$ (orange) forms fewer contacts than (CENP-A/H4)$_2$ (green) in the four-helix bundle region. The histogram of the number of contacts for (H3/H4)$_2$ has two peaks at 13 and 25 while (CENP-A/H4)$_2$ has a single peak at 27. The dash lines mark the four-helix contacts number in corresponding crystal structures. (B) Corresponding representative structures demonstrate that the (H3/H4)$_2$ four-helix bundle becomes broken or disrupted, while the four-helix bundle of (CENP-A/H4)$_2$ remains stable throughout our simulations. Four-helix bundles between two histone dimers are circled with dashed lines. αN and $\alpha N'$ helices are marked in green. The dimers of the H3 tetramer are shown in blue and red, and those of the CENP-A tetramer in cyan and orange.

Furthermore, we performed contact analysis for the four-helix bundle region. It demonstrates that there are more contacts, on average, in the corresponding region of (CENP-A/H4)$_2$ (~27) than in the same region of (H3/H4)$_2$ (~17) (Figure 5A). Also, one dominant peak is found in the (CENP-A/H4)$_2$ contacts histogram, but two peaks exist in that of (H3/H4)$_2$. Detailed residual

pair interactions from AWSEM show that the CENP-A residues Leu111, Gln127, and Arg131 contribute strong hydrophobic interactions to the four-helix bundle tetramer interface (Table S1), which H3 lacks. $(\text{CENP-A/H4})_2$ maintains a well-defined, native-like four-helix bundle throughout the simulation (Figure 5B), with the αN helices remaining outside the central interface. Note that the previously suggested CENP-A Leu112 residue(18), which is next to Leu111, is not found in the top strong interacting pairs of our simulations. The reason for this discrepancy is unclear.

Meanwhile, we observed structurally heterogeneous H3 αN helices, consistent with previous EPR experimental findings (54). Moreover, we notice that the αN sections of histone H3 may play an important role in disrupting the four-helix bundle at H3 tetrameric interface (Figure 5B & S11). Indeed, the distances between the αN helices from each H3 copy shows that the H3 αN helices feature a considerably wide distribution including two prominent peaks (at about 20 and 32 Å apart) (Figure S7D). Further, this disruption is mainly mediated through the hydrophobic interactions between Val46, Ala47, Leu48 from αN and Leu107, Ala111 from $\alpha 2$. The αN helix of H3 has greater hydrophobicity than CENP-A does, which could explain, in part, why H3 αN helices are more likely to be found close together at the interior of the tetramer than the same helices of CENP-A. We tested this hypothesis by performing similar simulations for both systems but starting from structures excluding αN helices. The analyses (Supplemental Section 10) confirmed our hypothesis that the flexible αN helices play a significant role in the swiveling motion of H3 tetramer, since switching between different H3 tetrameric dihedrals is significantly diminished when αN helices are excluded (Figure S10D). Interestingly, even without αN helices, CENP-A still forms more four-helix contacts (Figure S10B) and a more native-like binding interface (Figure S10C) than the H3 tetramer.

Hence, from this analysis we suggest that: (1) the unique hydrophobic residues (Leu112, Thr113, Leu114, Val126) at the CENP-A:CENP-A interface may help contribute an intrinsically stronger four-helix bundle than H3 specifically in the tetramer context; (2) the more hydrophobic H3 αN helix (Val46, Ala47, Leu48) tends to disrupt the relatively weak four-helix bundle formation and lead to the swiveling motion around the H3 tetramer interface.

Effects of H2A/H2B on histone tetramers

Finally, we wanted to examine the effects of histone dimer H2A/H2B on the dynamics of tetramers $(\text{H3/H4})_2$ and $(\text{CENP-A/H4})_2$. We investigated the DNA-free canonical H3 and variant CENP-A octamers using similar simulation procedures. Both the H2A/H2B dimers maintained well-native conformations throughout the simulations (Figure S11D). However, their distances to the central tetramer are diverse for H3 and CENP-A cases (Figure S11C), implying different effects of H2A/H2B to each tetramer.

As done for tetramers, similar analyses such as R_{COM}, R_g, and tetrameric dihedral θ were performed to explore the dynamics features of the histone octamers. For the H3 octamer, the distribution of both the tetrameric R_g and the distance R between H3/H4 pairs becomes more focused and Gaussian-like, compared to the *solo* tetramer situation (*solo* refers to the tetramer in isolation, without any other proteins; Figure 6A vs Figure 3B; Figure S11B vs Figure S7B). The standard deviation decreases from 3.8 Å to 1.9 Å for R, and from 1.4 Å to 0.7 Å for R_g, agreeing with previous EPR experimental data (54) showing the reduced H3 tetramer flexibility in an octamer. The distribution of the tetrameric dihedral angles of H3 features a dominant peak at 90° (Figure 6B), similar to that measured in the case of CENP-A, with the other two populations observed in *solo* H3 tetramer simulations diminished. 84% of H3 tetramer conformations in the octamer simulations have a positive tetrameric dihedral angle, significantly more than that in the *solo* tetramer simulations (58%). These data establish that the swiveling motion around the binding interface was reduced due to the bracketing histone dimers H2A/H2B on either side of the tetramer.

Nevertheless, analogous stabilizing effects were not found in the CENP-A octamer case. Interestingly, for the CENP-A octamer, a shoulder and a tail are present in the distributions of R and R_g of the CENP-A tetramer, indicating new conformational flexibility of $(\text{CENP-A/H4})_2$ in the context of an octamer. In particular, the second most populated state has a larger R_g and R than the dominant values observed for the *solo* CENP-A tetramer (Figure 6A vs Figure 3B; Figure S11B vs Figure S7B). In turn, this implies that the addition of H2A/H2B dimers leads to a less compact association of CENP-A dimers, encouraging the CENP-A tetramer to adopt a geometry closer to that found in the octameric nucleosome. This frustration between the intrinsic compactness of the *solo* CENP-A tetramer and the expansion and structural twisting induced by the addition of H2A/H2B dimers explains well the observed computational and experimental findings that CENP-A-containing histone nucleosomes or octamers are structurally more flexible and heterogeneous than their canonical counterparts (41, 42).

DISCUSSION

Maturation of the nucleosome stepping through dimers, tetramers, and octamers

In this work, we used coarse-grained modeling to study the thermodynamical and dynamical properties of canonical and variant CENP-A tetramers and octamers. Our results are largely in agreement with the prior experimental observations on these systems (H3 tetramer(51, 52) and octamer(54), H3 tetrasome(5) and CENP-A tetramer(18, 36)), providing important structural and

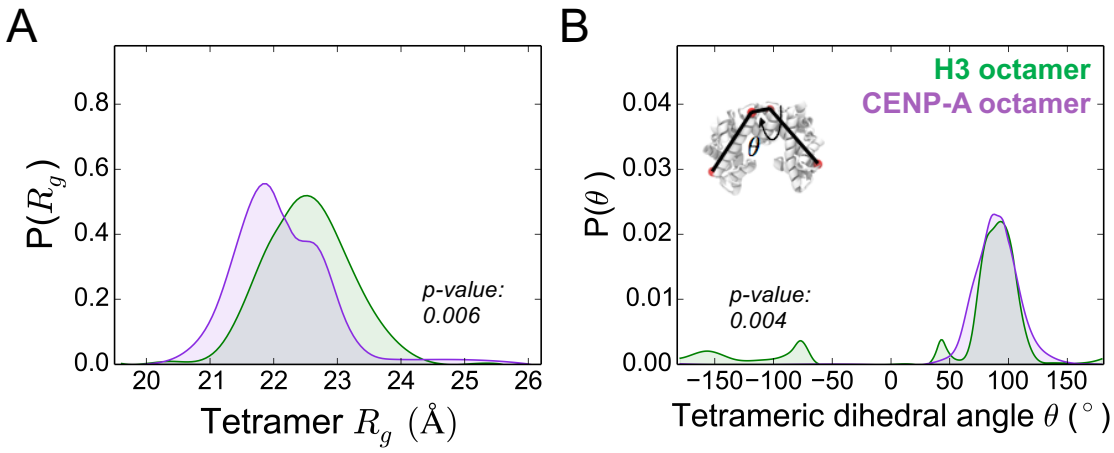

Figure 6: **H2A/H2B stabilizes (H3/H4)$_2$ but not (CENP-A/H4)$_2$.** (A) The probability distribution of H3 tetramer R_g features a more focused peak in the context of an octamer compared to that of the *solo* H3 tetramer (Figure 3C), while one peak and one shoulder exist in the same distribution for the CENP-A tetramer in the context of an octamer. (B) Distributions of the dihedral angle between $\alpha 2$ helices demonstrate that, in the presence of H2A/H2B, (H3/H4)$_2$ becomes more similar to (CENP-A/H4)$_2$; both curves feature a prominent peak around 80°.

dynamical details. In this study we focused on the fundamental mechanisms governing the histone oligomerization, hence the surrounding DNA and histone tails were not included in the simulations. In particular, since the histone tails are mainly disordered coils which may enhance the strucutal hetergeneity of the tetramer, their inclusion is expected to result in a relatively shallower free energy minimum, compared with our current results with tailess histones. Enhanced sampling techniques have been used in the past to study elements of transient structure in histone terminal tails with all-atom MD (60, 61). The effects of such tails and DNA on histone tetramers and octamers is an important future avenue of research.

Using both atomistic and coarse-grained simulations, we previously reported that, in the context of a dimer, histone H4 is more native-like than its binding partner H3 or CENP-A, and that the CENP-A/H4 dimer is more dynamic than its canonical counterpart (40). Here in the context of a tetramer, analyses of the monomer and dimer components yielded consistent results (see Supplemental Section 12). For instance, the average $Q_{monomer}$ for H4 is larger than that of H3 or CENP-A (Figure S13), implying its noticeable stability; Q_{dimer} and $Q_{dimer,interface}$ for H3 are larger, on average, than for CENP-A (Figure S12), indicating that H3 dimers adopt more native-like conformations than CENP-A dimers. However, compared to the structural variabilities within the dimer level, the movements between dimers forming the tetramer are on a larger scale, with an RMSD of 10~15 Å for the tetramer (Figure S7A) versus 3~4 Å for the dimer (Figure S12B, and Figure 2 in ref. 40). Therefore, the dynamics observed here by coarse-grained modeling are unlikely to be sampled ergodically using present-day atomistic simulations.

In our earlier study, the CENP-A nucleosome was shown to be more flexible than the H3 nucleosome, revealing to a shearing motion at the tetramer interface (41). Here, in the context of an octamer with H2A/H2B dimers, the CENP-A tetramer occupies two distinct conformational states: one that is similar to that of the isolated tetramer conformation, while the other state is less compact, structurally similar to the H3 (or CENP-A) tetramer in the context of the nucleosomal structure. Therefore, disrupting the energetically stable interface of the CENP-A tetramer likely underpins the shearing motion observed in the octameric CENP-A nucleosome. The two-state memory of the CENP-A tetramer in the octamer may explain why the CENP-A nucleosome is more distortable and dynamic compared with the canonical one.

Biological implications

We suggest several potential biological implications of our investigation. First, this work emphasizes the importance of structural context for the canonical H3 tetramer, which, *in vivo*, interacts with the surrounding DNA, histone (H2A/H2B)s, or chaperone proteins. The canonical tetramer may have evolved to be unstable, and highly dependent on other structural partners, which may be key to ensure the fidelity and stability of genetic material. On the other hand, CENP-A, as a functional variant histone, is intrinsically more stable in its tetramer form, and is therefore less dependent on DNA or other proteins, which may fit better its unique assembly pathway and intricate regulation.

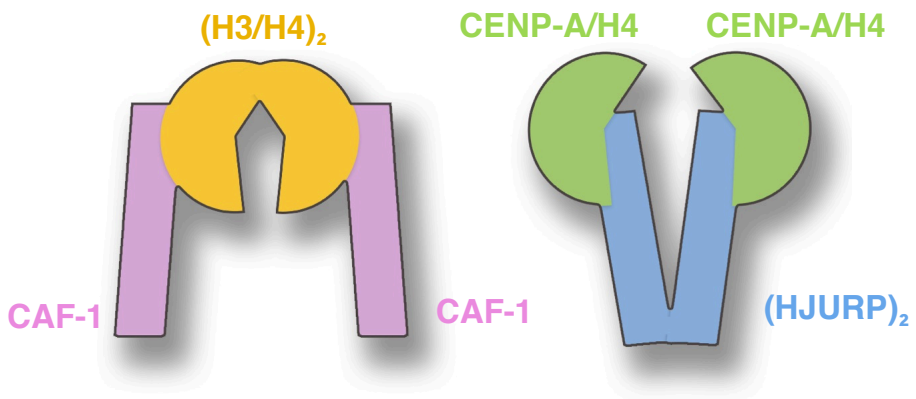

Figure 7: **Suggested models for histones and their chaperones during deposition.** (Left) H3/H4 may be deposited in the form of a tetramer with each external side bracketed by a CAF-1 chaperone, which may stabilize the tetramer. (Right) CENP-A may be deposited as dimers; each dimer loaded by one HJURP chaperone.

On the basis of our calculations, we speculate that the stably formed CENP-A tetramer could regulate the availability of individual CENP-A dimers, which we previously found to be flexible and could easily encounter other proteins (40). The rigidity of the CENP-A tetramer could prevent CENP-A from associating with non-centromeric proteins, so as to avoid the ectopic localization, or promiscuous interactions that might be more frequently occurring in cancer cells when CENP-A is over-expressed. A speculative proposal is that the $(\text{CENP-A/H4})_2$ tetramer may serve as a sequestration channel, needed to maintain CENP-A homeostasis. Indeed, one logical prediction is that histone modification in CENP-A, especially at the interface, which would either strengthen or weaken the rigidity/compactness of the tetramer, might influence the levels of dimer CENP-A/H4 available for chaperone-mediated assembly.

Another hypothesis based on this research is that the tetramerization of two CENP-A dimers could be nearly irreversible, so that the CENP-A tetramer, once formed, may not be able to separate into two dimers afterwards, even in the presence of chaperone HJURP (more simulation results about HJURP are in section S11). In this scenario, the DNA-free protein tetramer might serve as a kinetic trap for excess CENP-A. This hypothesis sheds light on the unique assembly/disassembly pathway of the CENP-A nucleosome. The CENP-A tetramer may be just one state along the assembly pathway of CENP-A nucleosome, after being delivered by HJURP, given the experimental evidence that the CENP-A–CENP-A′ interface is a requirement for stable chromatin incorporation (62).

The CENP-A-specific chaperone HJURP may block CENP-A dimers from self-associating into a tetramer by competing for the same binding site, the internal side of the CENP-A tetramer. It has been shown that two HJURP chaperones (63) and the dimerization of HJURP (64) is required for proper CENP-A nucleosome assembly. Therefore, a HJURP dimer may interact with two isolated CENP-A dimers, instead of with a CENP-A tetramer (Figure 7, right). On the contrary, as in the structure of H3 and its chaperone CAF-1 (65, 66), CAF-1 binds with an H3 dimer at the external side, without the possibility of preventing it from forming a tetramer. Indeed, the kinetically less stable tetramer of H3 may need the enhanced stabilization *via* binding with CAF-1 chaperones at either side (Figure 7, left). Taken all together, we propose two different chaperone models for CENP-A and H3 assembly, CENP-A/H4–$(\text{HJURP})_2$–CENP-A/H4 vs CAF-1–$(\text{H3/H4})_2$–CAF-1 (Figure 7), with a subtle yet important difference: in the former, two copies of HJURP would prevent two CENP-A dimers from forming a tetramer in pre-assembly complexes, whereas, in the latter, CAF-1 proteins would stabilize a pre-formed H3 tetramer in preparation for subsequent nucleosome assembly. Our results support the possibility that canonical H3- and CENP-A-containing nucleosomes may have orthogonal assembly pathways: while H3 could be deposited as a tetramer, CENP-A may be loaded in the form of a dimer.

CONCLUSION

This work establishes that variant histone CENP-A thermodynamically favors a tetramer formation while the canonical H3 presents remarkable rotation dynamics about the tetramer interface contributing a rugged yet shallow binding free energy landscape. Moreover, H2A/H2B dimers restrain the internal motion of $(\text{H3/H4})_2$ and lead to multiple states for $(\text{CENP-A/H4})_2$, providing a possible physical explanation for the shearing motion observed for the CENP-A nucleosome (41). These findings provide comprehensive molecular insights into the longstanding and recent experimental observations, offering a new perspective on the structural debates over CENP-A dynamics. Based on our results, we suggest two different assembly models for H3

and CENP-A. Lastly, we propose that the (CENP-A/H4)$_2$ tetramer may serve as a sequestration channel *in vivo*, which would provide another layer of regulation to ensure the proper homeostasis of CENP-A.

AUTHOR CONTRIBUTIONS

H.Z., Y.D. and G.P. designed the research. H.Z. carried out all simulations, analyzed the data. All authors wrote the article.

ACKNOWLEDGMENTS

H.Z. thanks Drs. Aram Davtyan and Bin Zhang for helpful discussions of AWSEM method, and Drs. Minh Bui, Ignacia Echeverria and Longhua Hu for critical reading of the manuscript. This work was supported by the National Science Foundation Grant NSF CHE-1363081 and the intramural research program of CCR/NCI. H.Z. is also supported by the Ann G. Wylie Dissertation Fellowship from the University of Maryland.

REFERENCES

1. Luger, K., A. W. Mader, R. K. Richmond, D. F. Sargent, and T. J. Richmond, 1997. Crystal structure of the nucleosome core particle at 2.8 A resolution. *Nature* 389:251–260.

2. Bina-Stein, M., and R. T. Simpson, 1977. Specific folding and contraction of DNA by histones H3 and H4. *Cell* 11:609–618.

3. Sollner-Webb, B., R. D. Camerini-Otero, and G. Felsenfeld, 1976. Chromatin structure as probed by nucleases and proteases: Evidence for the central role of hitones H3 and H4. *Cell* 9:179–193.

4. Vlijm, R., M. Lee, O. Ordu, A. Boltengagen, A. Lusser, N. H. Dekker, and C. Dekker, 2015. Comparing the assembly and handedness dynamics of (H3. 3-H4) 2 tetrasomes to canonical tetrasomes. *PloS one* 10:e0141267.

5. Vlijm, R., M. Lee, J. Lipfert, A. Lusser, C. Dekker, and N. H. Dekker, 2015. Nucleosome assembly dynamics involve spontaneous fluctuations in the handedness of tetrasomes. *Cell reports* 10:216–225.

6. Ordu, O., L. Kremser, A. Lusser, and N. H. Dekker, 2018. Modification of the histone tetramer at the H3-H3 interface impacts tetrasome conformations and dynamics. *The Journal of Chemical Physics* 148:123323.

7. Henikoff, S., T. Furuyama, and K. Ahmad, 2004. Histone variants, nucleosome assembly and epigenetic inheritance. *Trends Genet.* 20:320–326.

8. Sarma, K., and D. Reinberg, 2005. Histone variants meet their match. *Nat. Rev. Mol. Cell Bio.* 6:139–149.

9. Melters, D. P., J. Nye, H. Zhao, and Y. Dalal, 2015. Chromatin dynamics in vivo: a game of musical chairs. *Genes* 6:751–776.

10. Biterge, B., and R. Schneider, 2014. Histone variants: key players of chromatin. *Cell Tissue Res.* 356:457–466.

11. Sathyan, K. M., D. Fachinetti, and D. R. Foltz, 2017. α-amino trimethylation of CENP-A by NRMT is required for full recruitment of the centromere. *Nature Communications* 8:14678.

12. Bloom, K., and V. Costanzo, 2017. Centromere Structure and Function. *In* Centromeres and Kinetochores, Springer, 515–539.

13. Dalal, Y., T. Furuyama, D. Vermaak, and S. Henikoff, 2007. Structure, dynamics, and evolution of centromeric nucleosomes. *Proc. Natl. Acad. Sci. U. S. A.* 104:15974–15981.

14. Stankovic, A., L. Y. Guo, J. F. Mata, D. L. Bodor, X.-J. Cao, A. O. Bailey, J. Shabanowitz, D. F. Hunt, B. A. Garcia, B. E. Black, and L. E. Jansen, 2016. A dual inhibitory mechanism sufficient to maintain cell-cycle-restricted CENP-A assembly. *Molecular Cell* .

15. Nechemia-Arbely, Y., D. Fachinetti, K. H. Miga, N. Sekulic, G. V. Soni, D. H. Kim, A. K. Wong, A. Y. Lee, K. Nguyen, C. Dekker, B. Ren, B. E. Black, and D. W. Cleveland, 2017. Human centromeric CENP-A chromatin is a homotypic, octameric nucleosome at all cell cycle points. *J Cell Biol* 216:607–621.

16. Wang, K., Z. Yu, Y. Liu, and G. Li, 2017. Ser68 Phosphorylation Ensures Accurate Cell-Cycle-Dependent CENP-A Deposition at Centromeres. *Developmental Cell* 40:5–6.

17. Bui, M., M. Pitman, A. Nuccio, S. Roque, P. G. Donlin-Asp, A. Nita-Lazar, G. A. Papoian, and Y. Dalal, 2017. Internal modifications in the CENP-A nucleosome modulate centromeric dynamics. *Epigenetics & chromatin* 10:17.

18. Sekulic, N., E. A. Bassett, D. J. Rogers, and B. E. Black, 2010. The structure of (CENP-A-H4)(2) reveals physical features that mark centromeres. *Nature* 467:347–351.

19. Shivaraju, M., J. R. Unruh, B. D. Slaughter, M. Mattingly, J. Berman, and J. L. Gerton, 2012. Cell-cycle-coupled structural oscillation of centromeric nucleosomes in yeast. *Cell* 150:304–316.

20. Bui, M., E. K. Dimitriadis, C. Hoischen, E. An, D. Quénet, S. Giebe, A. Nita-Lazar, S. Diekmann, and Y. Dalal, 2012. Cell-cycle-dependent structural transitions in the human CENP-A nucleosome in vivo. *Cell* 150:317–326.

21. Dalal, Y., H. Wang, S. Lindsay, and S. Henikoff, 2007. Tetrameric structure of centromeric nucleosomes in interphase Drosophila cells. *PLoS Biol.* 5:e218.

22. Hasson, D., T. Panchenko, K. J. Salimian, M. U. Salman, N. Sekulic, A. Alonso, P. E. Warburton, and B. E. Black, 2013. The octamer is the major form of CENP-A nucleosomes at human centromeres. *Nat. Struct. Mol. Biol.* 20:687–695.

23. Furuyama, T., C. A. Codomo, and S. Henikoff, 2013. Reconstitution of hemisomes on budding yeast centromeric DNA. *Nucleic Acids Res.* 41:5769–5783.

24. Tanaka, Y., H. Tachiwana, K. Yoda, H. Masumoto, T. Okazaki, H. Kurumizaka, and S. Yokoyama, 2005. Human centromere protein B induces translational positioning of nucleosomes on alpha-satellite sequences. *J. Biol. Chem.* 280:41609–18.

25. Williams, J. S., T. Hayashi, M. Yanagida, and P. Russell, 2009. Fission yeast Scm3 mediates stable assembly of Cnp1/CENP-A into centromeric chromatin. *Mol. Cell* 33:287–98.

26. Zhang, W., S. U. Colmenares, and G. H. Karpen, 2012. Assembly of Drosophila centromeric nucleosomes requires CID dimerization. *Mol. Cell* 45:263–269.

27. Kato, H., J. Jiang, B.-R. Zhou, M. Rozendaal, H. Feng, R. Ghirlando, T. S. Xiao, A. F. Straight, and Y. Bai, 2013. A conserved mechanism for centromeric nucleosome recognition by centromere protein CENP-C. *Science* 340:1110–1113.

28. Dechassa, M. L., K. Wyns, M. Li, M. A. Hall, M. D. Wang, and K. Luger, 2011. Structure and Scm3-mediated assembly of budding yeast centromeric nucleosomes. *Nat. Commun.* 2:313.

29. Foltz, D. R., L. E. Jansen, A. O. Bailey, J. R. Yates, E. A. Bassett, S. Wood, B. E. Black, and D. W. Cleveland, 2009. Centromere-specific assembly of CENP-a nucleosomes is mediated by HJURP. *Cell* 137:472–484.

30. Dunleavy, E. M., D. Roche, H. Tagami, N. Lacoste, D. Ray-Gallet, Y. Nakamura, Y. Daigo, Y. Nakatani, and G. Almouzni-Pettinotti, 2009. HJURP is a cell-cycle-dependent maintenance and deposition factor of CENP-A at centromeres. *Cell* 137:485–497.

31. Zasadzińska, E., M. C. Barnhart-Dailey, P. H. J. Kuich, and D. R. Foltz, 2013. Dimerization of the CENP-A assembly factor HJURP is required for centromeric nucleosome deposition. *EMBO J.* 32:2113–2124.

32. Tachiwana, H., S. Müller, J. Blümer, K. Klare, A. Musacchio, and G. Almouzni, 2015. HJURP Involvement in De Novo CenH3 CENP-A and CENP-C Recruitment. *Cell Rep.* 11:22–32.

33. Barnhart-Dailey, M. C., P. Trivedi, P. T. Stukenberg, and D. R. Foltz, 2017. HJURP interaction with the condensin II complex during G1 promotes CENP-A deposition. *Molecular Biology of the Cell* 28:54–64.

34. Athwal, R. K., M. P. Walkiewicz, S. Baek, S. Fu, M. Bui, J. Camps, T. Ried, M.-H. Sung, and Y. Dalal, 2015. CENP-A nucleosomes localize to transcription factor hotspots and subtelomeric sites in human cancer cells. *Epigenetics & chromatin* 8:2.

35. Lacoste, N., A. Woolfe, H. Tachiwana, A. V. Garea, T. Barth, S. Cantaloube, H. Kurumizaka, A. Imhof, and G. Almouzni, 2014. Mislocalization of the centromeric histone variant CenH3/CENP-A in human cells depends on the chaperone DAXX. *Mol. Cell* 53:631–644.

36. Black, B. E., D. R. Foltz, S. Chakravarthy, and K. Luger, 2004. Structural determinants for generating centromeric chromatin. *Nature* 430:578–582.

37. Black, B. E., M. A. Brock, S. Bédard, V. L. Woods, and D. W. Cleveland, 2007. An epigenetic mark generated by the incorporation of CENP-A into centromeric nucleosomes. *Proc. Natl. Acad. Sci. U. S. A.* 104:5008–5013.

38. Tachiwana, H., W. Kagawa, T. Shiga, A. Osakabe, Y. Miya, K. Saito, Y. Hayashi-Takanaka, T. Oda, M. Sato, S.-Y. Park, H. Kimura, and H. Kurumizaka, 2011. Crystal structure of the human centromeric nucleosome containing CENP-A. *Nature* 476:232–235.

39. Kurumizaka, H., N. Horikoshi, H. Tachiwana, and W. Kagawa, 2013. Current progress on structural studies of nucleosomes containing histone H3 variants. *Curr. Opin. Struct. Biol.* 23:109–115.

40. Zhao, H., D. Winogradoff, M. Bui, Y. Dalal, and G. A. Papoian, 2016. Promiscuous histone mis-assembly is actively prevented by chaperones. *Journal of the American Chemical Society* 138:13207–13218.

41. Winogradoff, D., H. Zhao, Y. Dalal, and G. A. Papoian, 2015. Shearing of the CENP-A dimerization interface mediates plasticity in the octameric centromeric nucleosome. *Sci. Rep.* 5:17038.

42. Falk, S. J., L. Y. Guo, N. Sekulic, E. M. Smoak, T. Mani, G. A. Logsdon, K. Gupta, L. E. Jansen, G. D. Van Duyne, S. A. Vinogradov, M. A. Lampson, and B. E. Black, 2015. CENP-C reshapes and stabilizes CENP-A nucleosomes at the centromere. *Science* 348:699–703.

43. Davey, C. A., D. F. Sargent, K. Luger, A. W. Maeder, and T. J. Richmond, 2002. Solvent mediated interactions in the structure of the nucleosome core particle at 1.9 a resolution. *J. Mol. Biol.* 319:1097–1113.

44. Wood, C. M., J. M. Nicholson, S. J. Lambert, L. Chantalat, C. D. Reynolds, and J. P. Baldwin, 2005. High-resolution structure of the native histone octamer. *Acta Crystallographica Section F: Structural Biology and Crystallization Communications* 61:541–545.

45. Wood, C. M., S. Sodngam, J. M. Nicholson, S. J. Lambert, C. D. Reynolds, and J. P. Baldwin, 2006. The oxidised histone octamer does not form a H3 disulphide bond. *Biochimica et Biophysica Acta (BBA)-Proteins and Proteomics* 1764:1356–1362.

46. Arents, G., R. W. Burlingame, B.-C. Wang, W. E. Love, and E. N. Moudrianakis, 1991. The nucleosomal core histone octamer at 3.1 A resolution: a tripartite protein assembly and a left-handed superhelix. *Proceedings of the National Academy of Sciences* 88:10148–10152.

47. Tsunaka, Y., Y. Fujiwara, T. Oyama, S. Hirose, and K. Morikawa, 2016. Integrated molecular mechanism directing nucleosome reorganization by human FACT. *Genes & development* 30:673–686.

48. Chen, S., A. Rufiange, H. Huang, K. R. Rajashankar, A. Nourani, and D. J. Patel, 2015. Structure–function studies of histone H3/H4 tetramer maintenance during transcription by chaperone Spt2. *Genes & development* 29:1326–1340.

49. Saredi, G., H. Huang, C. M. Hammond, C. Alabert, S. Bekker-Jensen, I. Forne, N. Reverón-Gómez, B. M. Foster, L. Mlejnkova, T. Bartke, P. Cejka, N. Mailand, A. Imhof, D. J. Patel, and A. Groth, 2016. H4K20me0 marks post-replicative chromatin and recruits the TONSL–MMS22L DNA repair complex. *Nature* 534:714.

50. Huang, H., C. B. Strømme, G. Saredi, M. Hödl, A. Strandsby, C. González-Aguilera, S. Chen, A. Groth, and D. J. Patel, 2015. A unique binding mode enables MCM2 to chaperone histones H3–H4 at replication forks. *Nature Structural and Molecular Biology* 22:618.

51. Banks, D. D., and L. M. Gloss, 2003. Equilibrium Folding of the Core Histones: the H3- H4 Tetramer Is Less Stable than the H2A- H2B Dimer. *Biochemistry* 42:6827–6839.

52. Banks, D. D., and L. M. Gloss, 2004. Folding mechanism of the (H3–H4) 2 histone tetramer of the core nucleosome. *Protein science* 13:1304–1316.

53. Baxevanis, A. D., J. E. Godfrey, and E. N. Moudrianakis, 1991. Associative behavior of the histone (H3-H4) 2 tetramer: dependence on ionic environment. *Biochemistry* 30:8817–8823.

54. Bowman, A., R. Ward, H. El-Mkami, T. Owen-Hughes, and D. G. Norman, 2009. Probing the (H3-H4) 2 histone tetramer structure using pulsed EPR spectroscopy combined with site-directed spin labelling. *Nucleic acids research* 38:695–707.

55. Davtyan, A., N. P. Schafer, W. Zheng, C. Clementi, P. G. Wolynes, and G. A. Papoian, 2012. AWSEM-MD: protein structure prediction using coarse-grained physical potentials and bioinformatically based local structure biasing. *J. Phys. Chem. B* 116:8494–8503.

56. Zhang, B., W. Zheng, G. A. Papoian, and P. G. Wolynes, 2016. Exploring the free energy landscape of nucleosomes. *Journal of the American Chemical Society* 138:8126–8133.

57. Kumar, S., J. M. Rosenberg, D. Bouzida, R. H. Swendsen, and P. A. Kollman, 1992. The weighted histogram analysis method for free-energy calculations on biomolecules. I. The method. *Journal of computational chemistry* 13:1011–1021.

58. Boresch, S., and M. Karplus, 1996. The Jacobian factor in free energy simulations. *The Journal of chemical physics* 105:5145–5154.

59. Takada, S., R. Kanada, C. Tan, T. Terakawa, W. Li, and H. Kenzaki, 2015. Modeling structural dynamics of biomolecular complexes by coarse-grained molecular simulations. *Accounts of chemical research* 48:3026–3035.

60. Winogradoff, D., I. Echeverria, D. A. Potoyan, and G. A. Papoian, 2015. The acetylation landscape of the H4 histone tail: disentangling the interplay between the specific and cumulative effects. *Journal of the American Chemical Society* 137:6245–6253.

61. Potoyan, D. A., and G. A. Papoian, 2012. Regulation of the H4 tail binding and folding landscapes via Lys-16 acetylation. *Proceedings of the National Academy of Sciences* 109:17857–17862.

62. Bassett, E. A., J. DeNizio, M. C. Barnhart-Dailey, T. Panchenko, N. Sekulic, D. J. Rogers, D. R. Foltz, and B. E. Black, 2012. HJURP uses distinct CENP-A surfaces to recognize and to stabilize CENP-A/histone H4 for centromere assembly. *Dev. Cell* 22:749–762.

63. Bodor, D. L., and L. E. Jansen, 2013. How two become one: HJURP dimerization drives CENP-A assembly. *The EMBO journal* 32:2090–2092.

64. Zasadzińska, E., M. C. Barnhart-Dailey, P. H. J. Kuich, and D. R. Foltz, 2013. Dimerization of the CENP-A assembly factor HJURP is required for centromeric nucleosome deposition. *The EMBO journal* 32:2113–2124.

65. Liu, W. H., S. C. Roemer, Y. Zhou, Z.-J. Shen, B. K. Dennehey, J. L. Balsbaugh, J. C. Liddle, T. Nemkov, N. G. Ahn, K. C. Hansen, J. K. Tyler, and M. E. Churchill, 2016. The Cac1 subunit of histone chaperone CAF-1 organizes CAF-1-H3/H4 architecture and tetramerizes histones. *eLife* 5:e18023.

66. Mattiroli, F., Y. Gu, T. Yadav, J. L. Balsbaugh, M. R. Harris, E. S. Findlay, Y. Liu, C. A. Radebaugh, L. A. Stargell, N. G. Ahn, I. Whitehouse, and K. Luger, 2017. DNA-mediated association of two histone-bound CAF-1 complexes drives tetrasome assembly in the wake of DNA replication. *eLife* 6:e22799.